Journal of Power Sources 261 (2014) 101–111

Contents lists available at ScienceDirect

Journal of Power Sources

journal homepage: www.elsevier.com/locate/jpowsour

Parametric reduced-order models of battery pack vibration including structural variation and prestress effects

Sung-Kwon Hong [a,*], Bogdan I. Epureanu [a,*], Matthew P. Castanier [b]

[a] Department of Mechanical Engineering, University of Michigan, 2350 Hayward Street, Ann Arbor, MI 48109-2125, USA
[b] U.S. Army Tank Automotive Research, Development, and Engineering Center, Warren, MI 48397-5000, USA

HIGHLIGHTS

- Effect of prestress and cell-to-cell parameter variations in HEV battery pack are investigated.
- Novel numerical methods are developed for the HEV battery pack having high modal density.
- Monte Carlo simulations are performed to examine the effects of cell-to-cell variations.

ARTICLE INFO

Article history:
Received 13 November 2013
Received in revised form
18 February 2014
Accepted 5 March 2014
Available online 25 March 2014

Keywords:
Battery packs
Fatigue life predictions
Prestress
Cell-to-cell parameter variations
High modal density
Parametric reduced-order models

ABSTRACT

The goal of this work is to develop a numerical model for the vibration of hybrid electric vehicle (HEV) battery packs to enable probabilistic forced response simulations for the effects of variations. There are two important types of variations that affect their structural response significantly: the prestress that is applied when joining the cells within a pack; and the small, random structural property discrepancies among the cells of a battery pack. The main contributions of this work are summarized as follows. In order to account for these two important variations, a new parametric reduced order model (PROM) formulation is derived by employing three key observations: (1) the stiffness matrix can be parameterized for different levels of prestress, (2) the mode shapes of a battery pack with cell-to-cell variation can be represented as a linear combination of the mode shapes of the nominal system, and (3) the frame holding each cell has vibratory motion. A numerical example of an academic battery pack with pouch cells is presented to demonstrate that the PROM captures the effects of both prestress and structural variation on battery packs. The PROM is validated numerically by comparing full-order finite element models (FEMs) of the same systems.

1. Introduction

Typical hybrid electric vehicle (HEV) battery packs are assembled by bolts or welds for joining cells within the pack and for integrating the battery structure into the rest of the vehicle. The prestress due to joining can affect the dynamic response of the structures significantly. In addition, HEV battery pack structures typically include dozens or even hundreds of cells. Because the cells are nominally identical, if the cells are arranged in a spatially repeating layout then the battery pack falls under the class of structures known as periodic structures. The dynamics of periodic structures are known to feature very high modal density in many frequency bands. The high modal density combined with small, random structural variations among the cells (which are unavoidable in practice) can lead to drastic consequences on the structural dynamics. In particular, they can exhibit Anderson localization [1–3], where the vibration energy is spatially confined to a small region of the structure.

The focus of this work is to develop computationally efficient methods for predicting the vibratory response of a battery pack that may suffer from localization. It is believed that certain battery packs, such as those with pouch cells, may be especially susceptible to localization phenomena. Localization can lead to battery cell damage due to sharp increases in local vibration amplitude and stress levels in a pack, which in turn can lead to mechanical or electromechanical failure.

Stress and failure issues in battery packs have been investigated in several previous studies. For example, Offer et al. [4] provided a new concept of module design and a fault diagnosis technique in

* Corresponding authors. Tel.: +1 734 647 6391; fax: +1 734 764 4256.
E-mail addresses: sungkwon@umich.edu, hsungkwon@gmail.com (S.-K. Hong), epureanu@umich.edu (B.I. Epureanu), matt.castanier@us.army.mil (M.P. Castanier).

http://dx.doi.org/10.1016/j.jpowsour.2014.03.008
0378-7753/

electric vehicle batteries. They focused on testing the full battery pack and diagnosing subsequent problems related to cells to demonstrate how a full vehicle test can be used to identify malfunctioning strings of cells. Xiao et al. [5] developed a multi-scale approach for the stress analysis of polymeric separators in a lithium-ion battery. They presented a finite element method based on a multi-scale approach for the stress analysis of the separator in a battery cell. Sahraei et al. [6] revealed the underlying physics and identified important groups of parameters. To do that, they performed tests on pouched and bare lithium-ion cells under several loading conditions. They validated the test by numerical simulations. The outcomes from the test data were used for the development of an advanced constitutive model needed for strength/weight optimization and safety assessments of Li-ion batteries. Kenney et al. [7] established the relationship between cell-to-cell variations due to their manufacturing process and their overall impact on a full battery pack. They used mathematical modeling techniques to predict how slight variations in the manufacturing of electrodes manifest themselves in an operational battery module. The variation in the performance of the module has been quantified as a function of the manufacturing variation at the electrode level. Dubarry et al. [8] developed modeling and simulation techniques to show that accurate battery pack simulations can be achieved if cell-to-cell variations are taken into account. They used an accurate single-cell model which was validated against experimental data to provide high fidelity pack simulation.

However, the structural characteristics of the entire battery pack with very high modal density have not been previously explored. Therefore, the literature does not address the possible occurrence or prediction of localization in battery packs due to random structural variations among the cells.

In order to properly account for the effects of random variations, statistical dynamic response calculations are needed. Such statistical calculations are hard to perform using linear methods because the mode shapes of a pack depend in a nonlinear fashion on the parameters of each cell. The alternative is to use sample-based statistical analyses, such as Monte Carlo simulations. However, typical finite element models (FEMs) of battery packs have several million degrees of freedom (DOF). Thus, the computational time for obtaining just a single sample can be on the order of a day. This may make it infeasible to perform Monte Carlo simulations with FEMs.

To overcome this issue, in the field of structural dynamic analysis, component mode synthesis (CMS) [9–15] is well established as an alternative to conventional FEMs with large numbers of DOF. CMS belongs to a wide class of domain decomposition techniques. In a CMS approach, the global structure is divided into several substructures, and the DOF of each individual substructure are reduced significantly. Then, the substructures are reconnected, and the dynamic response of the system is predicted very efficiently and accurately. However, classical CMS must be modified in order to account for parametric variability in the structure. Thus, alternate, design-oriented techniques have been developed. One such approach is to generate what is referred to as parametric reduced-order models (PROMs). PROMs were introduced initially by Balmés et al. [16,17] to avoid the expensive process of reanalysis of complex structures. In addition, several other PROM methods have been developed [18–22].

In particular, the multiple-component PROMs (MC-PROMs) [21] have been developed by the authors. MC-PROMs are well suited for the structure modeled with shell-type finite elements. However, MC-PROMs have several drawbacks, namely: (1) a numerical instability of system level matrices can be encountered due to the transformation matrix, (2) MC-PROMs do not capture well elemental level nonlinearities for thickness variations of brick type finite elements, and (3) the interface DOF are hard to reduce. Thus, the next-generation PROMs (NX-PROMs) technique have been developed recently to overcome these drawbacks [22]. The concepts used in NX-PROMs are applied herein to capture the prestress variations.

The PROM techniques are highly efficient methods for estimating the statistics of the structural dynamic response. However, for a structure with very high modal density, previously developed PROMs have to be modified to efficiently capture the dynamic response. In particular, such a modification can be similar to the component mode mistuning (CMM) [23] method. CMM was developed for predicting the dynamic response of bladed disks found in turbo-machinery. Typically, these bladed disks suffer from high modal density. Thus, small structural variations in the blades significantly affect the system-level dynamic response. Nonetheless, it has been shown that the mode shapes of a mistuned bladed disk can be represented as a linear combination of the mode shapes of the tuned bladed disk [24]. This allows CMM to capture the dynamic response effectively with a small number of DOF, and that is the inspiration for the new PROMs introduced in this work.

This paper is organized as follows. In Section 2, structural properties and dynamic characteristics of HEV battery packs are evaluated. Next, in Section 3, PROM is applied for prestress variations, and new concept of PROM is developed for cell-to-cell structural variations. In Section 4, numerical examples of an academic battery pack models are used to demonstrate and test the proposed methods, including a Monte Carlo simulation technique that supports fatigue life prediction by quantifying stochastic effects in the forced response and sensitivities to various sources of parameter variation. Finally, conclusions are summarized in Section 5.

2. Structural properties and dynamic characteristics of battery packs

HEV battery packs typically have 100–300 individual cells that are nominally identical. To demonstrate the structural dynamic characteristics of a battery pack, a simplified academic model of a pack of pouch cells was developed using finite elements as shown in Fig. 1. The nodes on one end of the pack are totally fixed. The prestress and dynamic loads are applied to nodes on the other end of the structure. The prestress loads are applied to the longitudinal direction to compress the structure, and the harmonic excitations are applied to all three (x, y, z) directions. The excitation frequencies are in the range of 2200–2350 Hz. A total of 20 nominally identical cells are stacked. Typically, foam or epoxy stiffness layers can be placed between cells. These elements are nonlinear materials, but they are soft. Thus, herein these nonlinear materials are ignored.

To evaluate how the prestress variations in the structure affect the structural response, two different levels of prestress were applied: 150 kN and 470 kN. Fig. 2 shows the forced responses of the center node of the 1st cell for the different levels of prestress. The responses obtained by full-order models are significantly different for each level of prestress. For the prestress levels, the intent is to demonstrate that the PROMs can capture the structural dynamics for different prestress values that lead to a significant change in the forced response. The values 150 kN and 470 kN were chosen because they met these criteria for demonstrating the PROM performance. However, it should be noted that these are just two sampled prestress values, and the precise numbers do not have special significance.

Fig. 3 shows a single cell and the frames that join it to the adjacent cells. The single pouch cell is a plate-like structure for which the small, random structural variations are modeled by perturbations to the elastic modulus (E). The (nominally identical) cells are mechanically coupled through the frames, which induces a

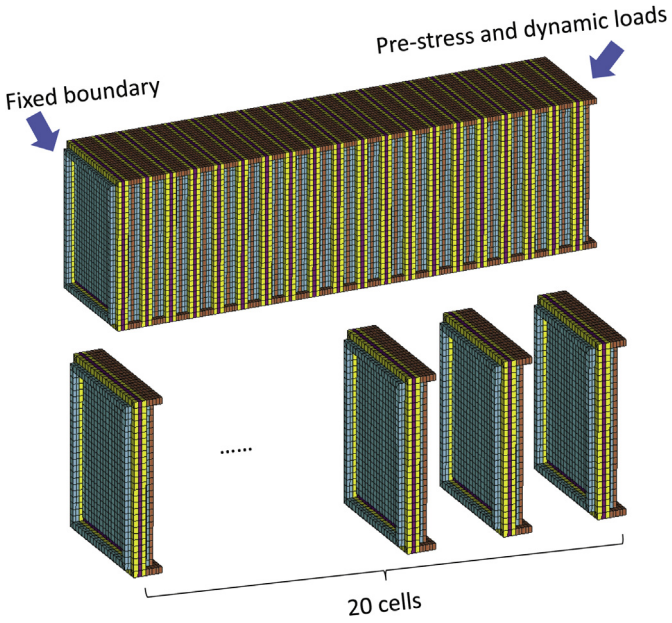

Fig. 1. The geometry of a battery pack with 20 pouch cells.

high modal density to the entire battery pack structure, as shown in Fig. 4. The flat regions in Fig. 4 indicate frequency ranges of high modal density. For example, there are over 20 modes in the range 2200–2300 Hz. If the battery pack had more cells, the modal density would be even higher. The frequency range 2200–2300 Hz features high modal density, as shown in Fig. 4. In such a frequency range, the forced response of a nominally periodic structure can be sensitive to small, random variations [2,3]. That is the reason for setting the excitation frequency in the range of 2200–2300 Hz. Note that there is also flat region of natural frequencies about 4000 Hz, and one would also expect to observe sensitivity of the forced response to parameter variation in this frequency range. However, for this academic example, there was no specific reason to examine a higher frequency range. Therefore, the lower frequency range was selected for this initial study.

To examine how structural variations in the cells affect the structural response, Young's modulus variations were applied, as

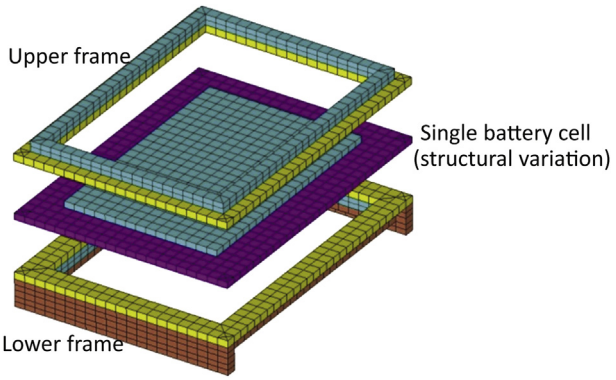

Fig. 3. The geometry of a single pouch cell.

described in Table 1. Young's modulus changes were used as a simple way to vary the cell stiffnesses directly in both the finite element model and the PROM. In practice, some small differences among the stiffnesses of the cells are unavoidable due to thickness variations and other manufacturing tolerances. In addition, even if each cell started perfectly identical, as the battery cells are charged and discharged they experience large temperature fluctuations, and the individual cell stiffnesses will vary accordingly during operation. Therefore, Young's modulus changes were used to model the overall variability in cell stiffnesses. Furthermore, in order to observe the consequences of small parameter variations in just a few cells, for cases 1 and 2 the variations were applied in only four cells. However, for other cases, the variations were applied to all cells, which is the more realistic case.

The mode shapes of the structure with nominal parameters (no variation) were compared with the mode shapes of the structure for cases 1 and 2. These mode shapes are shown in Fig. 5. Although the structural variations were small, the mode shapes are affected significantly. In particular, note that some mode shapes are localized about a few cells in which there are no parameter variations.

The forced response for the nominal case was also compared to the forced response for each case of variation, as shown in Fig. 6. These results show that small local structural variations can induce large changes in the global forced response. Fig. 6 shows the response of the 4th cell (top plot) and the 6th cell (bottom plot). As shown in Table 1, there are no variations in the parameters of cells 4

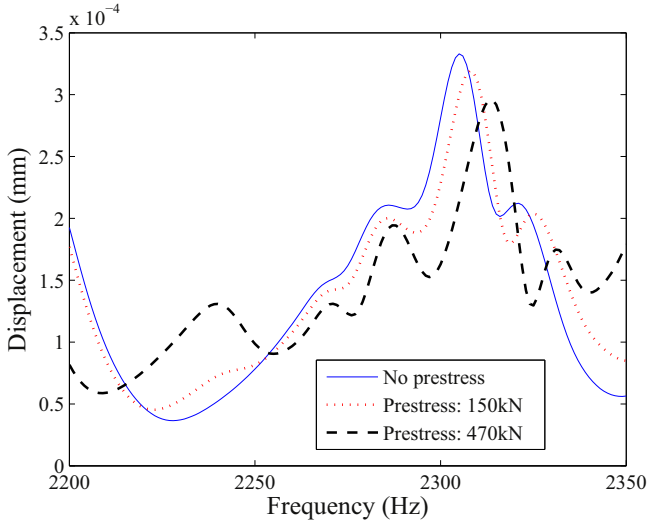

Fig. 2. Forced response of the center node of the 1st cell for different levels of prestress without structural variation.

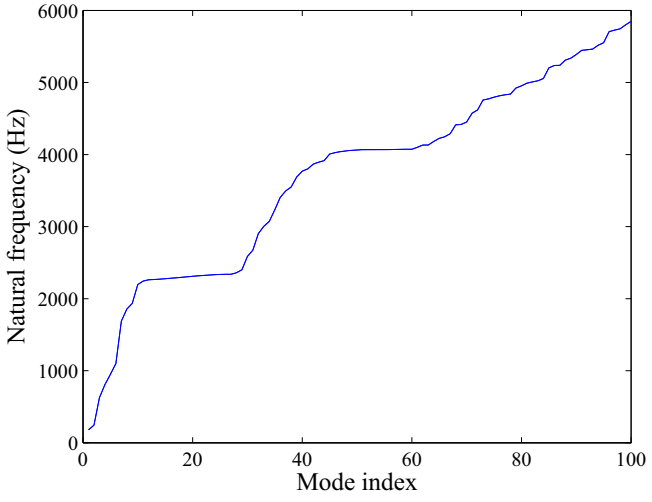

Fig. 4. Natural frequencies of the academic battery pack without prestress and without cell-to-cell variations.

Table 1
Two patterns of Young's modulus variations.

Pattern 1		Pattern 2	
Cell	Variation	Cell	Variation
1	5%	3	3%
5	−7%	9	−5%
12	1%	13	2%
16	3%	20	−5%

and 6. However, there are significant changes in the dynamic response of these cells. For example, the maximum response of the 6th cell is approximately 0.0085 mm, whereas the maximum response of the same cell in case 2 of parameter variations is approximately 0.0061 mm. This is almost a 30% increase in the maximum response, even though the maximum parameter variation between the nominal battery and that of case 2 is only 5%. This demonstrates that small local structural variations can have large global consequences. To efficiently capture the dynamic characteristics of the structure with simultaneous prestress and structural variations, a new approach was developed, as described in the next section.

3. Parametric reduced-order model

3.1. Modeling prestress in a structure

The prestress affects the dynamic response of structures by changing their stiffness. The first key idea of PROMs is the parameterization of the stiffness matrices [22]. The parameterization significantly reduces the reanalysis time because any variation in the parametric range can be applied for different levels of prestress without full-order finite element calculations or mesh refinement. The other key idea is to predict vibration responses using reduced-order models (ROMs) as opposed to full-order models to reduce the calculation time. To detail the construction of PROMs, these two key ideas are implemented.

The transformation matrix for PROMs is constructed by a set of fixed-interface normal modes $\mathbf{\Phi}^N_{\text{aug}}$ given by

$$\mathbf{\Phi}^N_{\text{aug}} = \left[\mathbf{\Phi}^N_0 \quad \mathbf{\Phi}^N_1 \quad \mathbf{\Phi}^N_2 \quad \mathbf{\Phi}^N_3\right],$$

where matrix $\mathbf{\Phi}^N_0$ corresponds to the nominal parameter values, and matrices $\mathbf{\Phi}^N_i$ $(i = 1, 2, 3)$ correspond to 3 other parameter values. A third-order interpolation is used for a parameterization. Thus, 4 samples of matrices (at distinct parameter values) are needed for constructing the transformation matrix.

In general, the columns of $\mathbf{\Phi}^N_{\text{aug}}$ are not orthogonal. Therefore, for numerical stability, an orthogonal basis for the space spanned by these modes is computed. This basis is obtained by a truncated set of left singular vector $\mathbf{U}^N$ of $\mathbf{\Phi}^N_{\text{aug}}$ [21,22]. The basis of vectors in $\mathbf{U}^N$ is orthogonal, so numerical conditioning problems are avoided. In addition, the left singular vectors $\mathbf{U}^N$ are truncated to lower the size of the resulting model. The choice of the cutoff point can affect accuracy if it is chosen too high, but it does not affect numerical stability. Thus, the cutoff value can be estimated by a standard convergence study where calculations are done at ever lower cutoff values until convergence is obtained. For the calculations performed in this study, the cutoff was 0.01% of the maximum singular value. Then $\mathbf{U}^N$ is used in a transformation matrix $\mathbf{T}^{\text{PROM}}$ to convert for physical coordinates to generalized coordinates. The transformed stiffness matrices for the 4 samples of such matrices

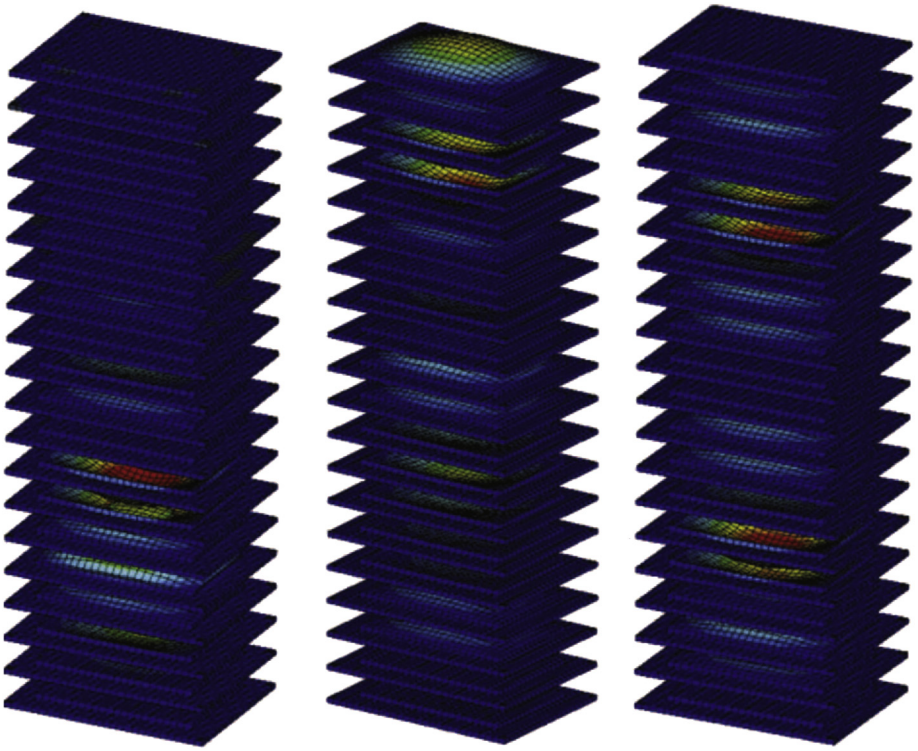

Fig. 5. Mode shapes of the nominal structure with identical cells (left) and the structures with cases 1 (center) and 2 (right) of cell parameter variations.

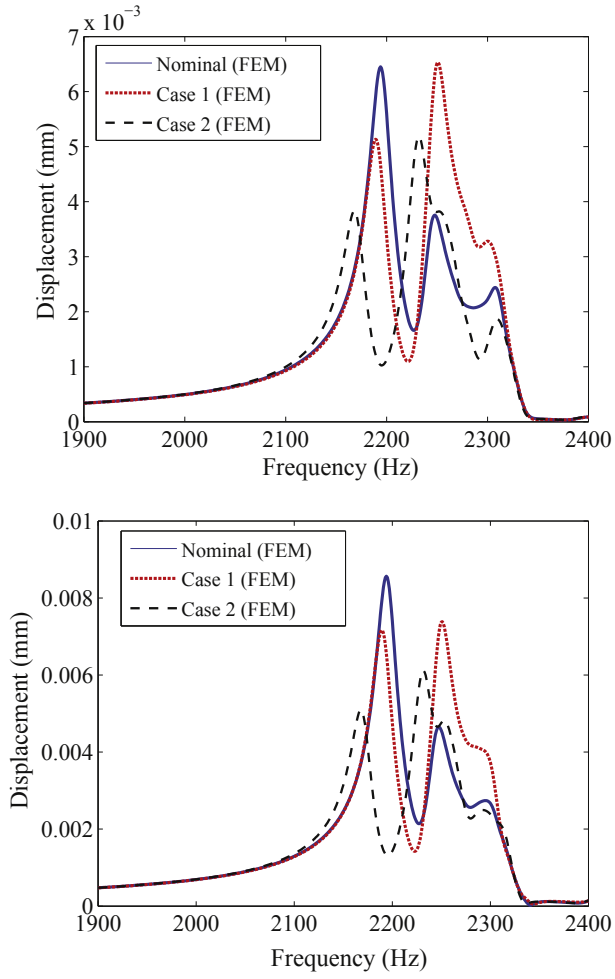

Fig. 6. Forced response of the center node of the 4th cell (top) and the 6th cell (bottom) for the nominal case of no parameter variations versus two cases with parameter variations.

$$\mathbf{K}_i^{\mathrm{PROM}} = \left(\mathbf{T}^{\mathrm{PROM}}\right)^{\mathrm{T}} \mathbf{K}_i^{\mathrm{FEM}} \mathbf{T}^{\mathrm{PROM}}, \tag{1}$$

where ($i = 0, 1, 2, 3$).

For convenience, the parameterization procedure is summarized next. This procedure closely follows that of Hong et al. [22]. The parameterization equation consists of a third-order interpolation, which can be written as

$$\mathbf{K}(p_0 + \Delta p) \approx \mathbf{K}_0 + \Delta p \mathbf{K}_1 + \Delta p^2 \mathbf{K}_2 + \Delta p^3 \mathbf{K}_3.$$

Four equations are needed to calculate the matrices $\mathbf{K}_i$ (for $i = 0, 1, 2, 3$). To obtain these four equations, reduced-order stiffness matrices are computed using Eq. (1) for four parameter values. First, consider the case where $\Delta p = 0$. One obtains

$$\mathbf{K}(p_0) \approx \mathbf{K}_0^{\mathrm{PROM}}. \tag{2}$$

Next, consider $\Delta p = i\delta p$ (with $i = 1, 2, 3$), one obtains

$$\mathbf{K}(p_0 + i\delta p) \approx \mathbf{K}_i^{\mathrm{PROM}} \approx \mathbf{K}_0 + (i\delta p)\mathbf{K}_1 + (i\delta p)^2 \mathbf{K}_2 + (i\delta p)^3 \mathbf{K}_3. \tag{3}$$

Rearranging Eqs. (2) and (3) into matrix form, for each entry e, q of the matrices $\mathbf{K}_0$, $\mathbf{K}_1$, $\mathbf{K}_2$ and $\mathbf{K}_3$, one obtains

$$\mathbf{C} \begin{bmatrix} \mathbf{K}_{0,\mathrm{eq}} \\ \mathbf{K}_{1,\mathrm{eq}} \\ \mathbf{K}_{2,\mathrm{eq}} \\ \mathbf{K}_{3,\mathrm{eq}} \end{bmatrix} = \begin{bmatrix} \mathbf{K}(p_0)_{\mathrm{eq}} \\ \mathbf{K}(p_0 + \delta p)_{\mathrm{eq}} \\ \mathbf{K}(p_0 + 2\delta p)_{\mathrm{eq}} \\ \mathbf{K}(p_0 + 3\delta p)_{\mathrm{eq}} \end{bmatrix}, \tag{4}$$

where

$$\mathbf{C} = \begin{bmatrix} 1 & 0 & 0 & 0 \\ 1 & \delta p & (\delta p)^2 & (\delta p)^3 \\ 1 & 2\delta p & (2\delta p)^2 & (2\delta p)^3 \\ 1 & 3\delta p & (3\delta p)^2 & (3\delta p)^3 \end{bmatrix}.$$

Equation (4) can be easily solved by simply inverting the 4×4 matrix $\mathbf{C}$. Let us denote by $\mathbf{A}$ this inverse matrix, i.e.

$$\mathbf{A} = \mathbf{C}^{-1} = \begin{bmatrix} \mathbf{A}_{11} & \mathbf{A}_{12} & \mathbf{A}_{13} & \mathbf{A}_{14} \\ \mathbf{A}_{21} & \mathbf{A}_{22} & \mathbf{A}_{23} & \mathbf{A}_{24} \\ \mathbf{A}_{31} & \mathbf{A}_{32} & \mathbf{A}_{33} & \mathbf{A}_{34} \\ \mathbf{A}_{41} & \mathbf{A}_{42} & \mathbf{A}_{43} & \mathbf{A}_{44} \end{bmatrix}.$$

Rearranging Eq. (4) using the entries $\mathbf{A}$, one obtains

$$\begin{aligned} \mathbf{K}(p_0 + \Delta p) &\approx \mathbf{K}_{\Delta p}^{\mathrm{PROM}} \\ &\approx b_0 \mathbf{K}_0^{\mathrm{PROM}} + b_1 \mathbf{K}_1^{\mathrm{PROM}} + b_2 \mathbf{K}_2^{\mathrm{PROM}} + b_3 \mathbf{K}_3^{\mathrm{PROM}}, \end{aligned} \tag{5}$$

where

$$\begin{aligned} b_0 &= (A_{11} + A_{21}\Delta p + A_{31}\Delta p^2 + A_{41}\Delta p^3), \\ b_1 &= (A_{12} + A_{22}\Delta p + A_{32}\Delta p^2 + A_{42}\Delta p^3), \\ b_2 &= (A_{13} + A_{23}\Delta p + A_{33}\Delta p^2 + A_{43}\Delta p^3), \\ b_3 &= (A_{14} + A_{24}\Delta p + A_{34}\Delta p^2 + A_{44}\Delta p^3). \end{aligned}$$

The parameterized stiffness matrix in Eq. (5) is used to capture the dynamic response of the structure with different levels of prestress. Details of this procedure can be found also in Hong et al. [22].

This section described the way to capture the prestress effect efficiently based on NX-PROMs [22]. In the next section, the numerical methods to predict the dynamic response of the periodic structure which features very high modal density are formulated.

3.2. Modeling structural variations in cells

The equations of motion for the structure with no variation and with variation can be expressed as

$$\mathbf{M}\ddot{\mathbf{x}} + \mathbf{C}\dot{\mathbf{x}} + \mathbf{K}\mathbf{x} = \mathbf{F}, \tag{6}$$

$$\mathbf{M}\ddot{\mathbf{x}} + \mathbf{C}\dot{\mathbf{x}} + \left(\mathbf{K} + \mathbf{K}^{\delta}\right)\mathbf{x} = \mathbf{F}, \tag{7}$$

where $\mathbf{K}^{\delta}$ contains the stiffness variation. Based on Eqs. (6) and (7), the mode shapes are defined by the following eigenvalue problems

$$\begin{aligned} &\mathbf{K}\boldsymbol{\Phi}^t - \mathbf{M}\boldsymbol{\Phi}^t\boldsymbol{\Lambda}^t = 0, \\ &\left(\mathbf{K} + \mathbf{K}^{\delta}\right)\boldsymbol{\Phi}^m - \mathbf{M}\boldsymbol{\Phi}^m\boldsymbol{\Lambda}^m = 0, \end{aligned}$$

where superscript t and m indicate the tuned (nominal) and mistuned (structure with variation) quantities. Matrices $\boldsymbol{\Lambda}^t$ and $\boldsymbol{\Lambda}^m$ are diagonal and contain the eigenvalues of the tuned and mistuned systems. If the structure has mass variations, the mass matrix in Eq. (7) is $(\mathbf{M} + \mathbf{M}^{\delta})$. For the sake of simplicity, only the case of stiffness variations was considered.

The novel approach is based on two key assumptions. The first assumption is that the mode shapes $\boldsymbol{\Phi}^m$ of a pack with parametric

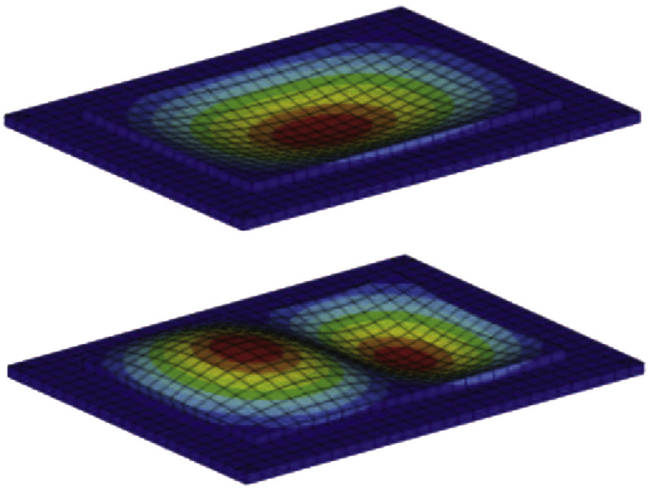

Fig. 7. 1st and 2nd modes of a fixed-boundary pouch cell.

variations can be approximated as a linear combination of the mode shapes $\mathbf{\Phi}^t$ of nominal pack with no parametric variations. This first assumption is ensured by the high modal density.

The second assumption for structural variations is that the variations in stiffness of a cell can be projected onto a small set of modes of the nominal cell with a fixed boundary, as shown in Fig. 7. This second assumption relies on the fact that the boundary motions can be ignored when the boundary of the pouch cell is not moving. However, it turns out that the boundary motion has to be considered because it is not small, as shown in Fig. 8. Thus, the plate-like modes of a nominal cell-with its boundary displaced the same amount as the frame-are used in the proposed PROMs. This is a key step for ensuring accuracy. This approach is distinct from the original CMM method [23] because the CMM method does not account for the boundary motion.

These two key ideas are implemented to model a system with prestress variations. Eq. (6) for the tuned (nominal) structure with prestress variations can be written as

$$\mathbf{M}^{\mathrm{PROM}}_{\Delta p,0}\ddot{\mathbf{u}}^{\mathrm{PROM}} + (1+j\gamma)\mathbf{K}^{\mathrm{PROM}}_{\Delta p,0}\mathbf{u}^{\mathrm{PROM}} = \mathbf{F}^{\mathrm{PROM}}, \tag{8}$$

where $\mathbf{u}^{\mathrm{PROM}}$ are generalized coordinates given by $\mathbf{x} = \mathbf{T}^{\mathrm{PROM}}\mathbf{u}^{\mathrm{PROM}}$. Subscript Δp indicates the prestress variation and subscript 0 indicates no structural variations. γ is a structural damping coefficient.

The eigenvalue problem determined from Eq. (8) with $\mathbf{F}^{\mathrm{PROM}} = 0$ is solved to determine the natural frequencies $\mathbf{\Lambda}^{\mathrm{PROM}}_{\Delta p,0}$ and mode shapes $\mathbf{\Phi}^{\mathrm{PROM}}_{\Delta p,0}$ of the system. Next, a secondary modal analysis can be used to transform coordinates from $\mathbf{u}^{\mathrm{PROM}}$ to $\mathbf{v}^{\mathrm{PROM}}$ such that $\mathbf{u}^{\mathrm{PROM}} = \mathbf{\Phi}^{\mathrm{PROM}}_{\Delta p,0}\mathbf{v}^{\mathrm{PROM}}$. Eq. (8) becomes

$$\ddot{\mathbf{v}}^{\mathrm{PROM}} + (1+j\gamma)\mathbf{\Lambda}^{\mathrm{PROM}}_{\Delta p,0}\mathbf{v}^{\mathrm{PROM}} = \left(\mathbf{\Phi}^{\mathrm{PROM}}_{\Delta p,0}\right)^{\mathrm{T}}\mathbf{F}^{\mathrm{PROM}}.$$

Note that $\mathbf{\Lambda}^{\mathrm{PROM}}_{\Delta p,0}$ contains eigenvalues of the prestressed structure without variation. That is different from $\mathbf{\Lambda}^t$ which contains eigenvalues of the tuned system without prestress.

As described above, the first key assumption is used in the PROM domain. The mistuned mode shapes of the structure can be represented as a linear combination of tuned mode shapes. Thus, one can assume the physical coordinates $\mathbf{x}$ in Eq. (7) can be expressed as

$$\mathbf{x} = \mathbf{T}^{\mathrm{PROM}}\mathbf{u}^{\mathrm{PROM}} = \mathbf{T}^{\mathrm{PROM}}\mathbf{\Phi}^{\mathrm{PROM}}_{\Delta p,0}\mathbf{v}^{\mathrm{PROM}}.$$

Then the equations of motion of the mistuned structure in the $\mathbf{v}^{\mathrm{PROM}}$ coordinates can be written as

$$\ddot{\mathbf{v}}^{\mathrm{PROM}} + (1+j\gamma)\left(\mathbf{\Lambda}^{\mathrm{PROM}}_{\Delta p,0}\mathbf{v}^{\mathrm{PROM}} + \mathbf{A}\right) = \left(\mathbf{\Phi}^{\mathrm{PROM}}_{\Delta p,0}\right)^{\mathrm{T}}\mathbf{F}^{\mathrm{PROM}},$$

where $\mathbf{A} = (\mathbf{\Phi}^{\mathrm{PROM}}_{\Delta p,0})^{\mathrm{T}}(\mathbf{T}^{\mathrm{PROM}})^{\mathrm{T}}\mathbf{K}^{\mathrm{FEM}}_{\Delta p,\delta}\mathbf{T}^{\mathrm{PROM}}\mathbf{\Phi}^{\mathrm{PROM}}_{\Delta p,0}\mathbf{v}^{\mathrm{PROM}}$, and $\mathbf{K}^{\mathrm{FEM}}_{\Delta p,\delta}$ contains the variations in the stiffness matrix in physical coordinates between the nominal structure and the structure with variations.

To parameterize the stiffness variation in the jth cell, a first-order interpolation was used, which is given by

$$\mathbf{K}^{\mathrm{FEM},j}_{\Delta p,\delta} = m_j\mathbf{K}^{\mathrm{FEM},j}_{\Delta p,0},$$

where $\mathbf{K}^{\mathrm{FEM},j}_{\Delta p,0}$ is the jth cell stiffness matrix for the nominal cell, and m_j is the amount of stiffness variations in the jth cell. Then $\mathbf{K}^{\mathrm{FEM},j}_{\Delta p,0}$ can be partitioned into

$$\mathbf{K}^{\mathrm{FEM},j}_{\Delta p,0} = \begin{bmatrix}\mathbf{K}^0_{AA} & \mathbf{K}^0_{AO}\\ \mathbf{K}^0_{OA} & \mathbf{K}^0_{OO}\end{bmatrix},$$

where subscript A and O are DOF refer to interface (A) and internal (O) DOF of the jth cell. The partitions of the stiffness matrix are used to calculate the static deformation from the boundary displacement of the jth cell by using

$$\begin{bmatrix}\mathbf{K}^0_{AA} & \mathbf{K}^0_{AO}\\ \mathbf{K}^0_{OA} & \mathbf{K}^0_{OO}\end{bmatrix}\begin{bmatrix}\overline{\mathbf{T}}_{A,j}\\ \overline{\mathbf{T}}_{O,j}\end{bmatrix} = \begin{bmatrix}\mathbf{F}_A\\ \mathbf{F}_O\end{bmatrix}, \tag{9}$$

where $\overline{\mathbf{T}}_{A,j}$ and $\overline{\mathbf{T}}_{O,j}$ are interface and internal displacements of the jth cell. The interface displacement $\overline{\mathbf{T}}_{A,j}$ is obtained from the transformation matrix $\mathbf{T}^{\mathrm{PROM}}$ by selecting entries corresponding to interface DOF of the jth cell from global DOF, which is

$$\overline{\mathbf{T}}_{A,j} = \mathbf{T}^{\mathrm{PROM}}_{A,j}.$$

Then the static deformation induced by the boundary displacement can be computed by Eq. (9), that is

$$\overline{\mathbf{T}}_j = \begin{bmatrix}\overline{\mathbf{T}}_{A,j}\\ \overline{\mathbf{T}}_{O,j}\end{bmatrix} = \begin{bmatrix}\mathbf{T}^{\mathrm{PROM}}_{A,j}\\ -\mathbf{K}^{0^{-1}}_{OO}\mathbf{K}^0_{OA}\mathbf{T}^{\mathrm{PROM}}_{A,j}\end{bmatrix}.$$

Next, a set of fixed interface normal modes $\mathbf{\Phi}^C$ of a single battery cell structure are calculated. The fixed-interface normal modes are a truncated set of modes obtained by solving the eigenproblem with the mass and stiffness matrices of the cell with a fixed boundary. One obtains

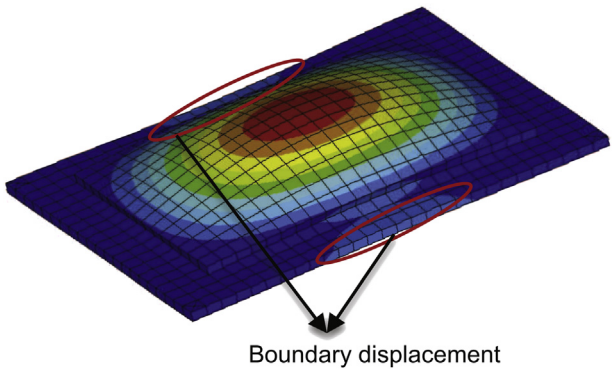

Fig. 8. Boundary-displaced motion of a pouch cell.

$$\mathbf{K}_{OO}^{0}\boldsymbol{\Phi}_{OO}^{C} - \mathbf{M}_{OO}^{0}\boldsymbol{\Phi}_{OO}^{C}\boldsymbol{\Lambda}^{C} = 0,$$

where $\boldsymbol{\Phi}^{C} = \left[\boldsymbol{\Phi}_{AA}^{C}/\boldsymbol{\Phi}_{OO}^{C}\right] = \left[0/\boldsymbol{\Phi}_{OO}^{C}\right]$.

Next, the computed static deformation $\overline{\mathbf{T}}_j$ and a set of fixed interface normal modes $\boldsymbol{\Phi}^{C}$ of the single cell are used to calculate modal participation factors $\mathbf{q}_j$ as follows

$$\mathbf{T}_j^{\mathrm{PROM}} - \overline{\mathbf{T}}_j = \boldsymbol{\Phi}^{C}\mathbf{q}_j,$$

$$\mathbf{q}_j = \left(\boldsymbol{\Lambda}^{C}\right)^{-1}\left(\boldsymbol{\Phi}^{C}\right)^{\mathrm{T}}\mathbf{K}_{\Delta p,\delta}^{FEM,j}\left(\mathbf{T}_j^{\mathrm{PROM}} - \overline{\mathbf{T}}_j\right).$$

These relations are used to construct the equations of motion for prestress and stiffness variations as follows

$$\ddot{\mathbf{v}}^{\mathrm{PROM}} + (1 + j\gamma)\boldsymbol{\Lambda}_{\Delta p,0}^{\mathrm{PROM}}\mathbf{v}^{\mathrm{PROM}} + \mathbf{B} = \left(\boldsymbol{\Phi}_{\Delta p,0}^{\mathrm{PROM}}\right)^{\mathrm{T}}\mathbf{F}^{\mathrm{PROM}},$$

where

$$\mathbf{B} = (1 + j\gamma)\left(\boldsymbol{\Phi}_{\Delta p,0}^{\mathrm{PROM}}\right)^{\mathrm{T}}\mathbf{C}\boldsymbol{\Phi}_{\Delta p,0}^{\mathrm{PROM}}\mathbf{v}^{\mathrm{PROM}},$$

$$\mathbf{C} = \left[\sum_{j=1}^{N}\left(\boldsymbol{\Phi}^{C}\mathbf{q}_j + \overline{\mathbf{T}}_j\right)^{\mathrm{T}}\mathbf{K}_{\Delta p,0}^{\mathrm{FEM},j}\left(\boldsymbol{\Phi}^{C}\mathbf{q}_j + \overline{\mathbf{T}}_j\right)\right],$$

and N is the number of cells that have stiffness variations.

The PROM for the HEV battery pack structure has been formulated to predict the dynamic response when the structure has a prestress and cell-to-cell variations. In the next section, the computational efficiency and accuracy of the newly developed PROM is evaluated by applying it to the academic battery pack.

4. Numerical results

As a benchmark for testing the performance of the proposed method, forced response results were been obtained using the academic battery finite element model shown in Fig. 1. This FEM has 208,753 DOF and features 20 nominally identical cells.

The frequency range of interest is 1500–3000 Hz, which is the first flat region of the natural frequencies plotted in Fig. 4. This type of frequency band with high modal density is characteristic of periodic structures. For system modes in such a region, the vibration response shape of each cell will tend to be very close to that of a mode shape for a single, isolated cell. For this particular band of system modes, the response shape of each cell is very close to the first fixed-boundary mode shape of a cell, which is the top mode shape shown in Fig. 7.

Prestress and dynamic loads were applied as shown in Fig. 1. For the dynamic loads, harmonic forcing was applied at the right end (cell 20) while the boundary DOF at the left end (cell 1) were held fixed. For this initial study, both the model and the loading were intentionally kept simple. More realistic models and loading conditions will be examined in future work.

For the following numerical results, the forced response amplitudes were obtained at the center nodes of the cells. As with the free response, the forced response shape of each cell was very close to the first mode shape of an individual cell (multiplied by a scalar amplitude), based on direct observation of the finite element analysis results. In particular, the response shape of each cell was similar to that of the first fixed-boundary mode shape. (It is recognized that this might lead one to assume that each cell will not interact dynamically with neighboring cells. However, it should be noted that the boundary—the frame—is not fixed. In fact, the frame vibrates and provides significant dynamic coupling among the cells.) Therefore, the maximum forced response displacement for each cell occurred at the center node. Furthermore, the amplitudes at the center nodes of the cells are representative of not only the maximum displacement levels but also the maximum stress levels of the cells. Therefore, the effects of prestress and structural variation on these amplitudes provide an excellent indicator of the effects on fatigue life. Higher amplitudes indicate correspondingly higher stresses as well as an increased risk of structural fatigue failure.

Table 2
Comparison of the full-order models and the PROM.

	Full-order model	PROM
System DOF	208,753	38
Reanalysis time	10,120–10,780 s	0.89–0.95 s

4.1. Validation of PROM performance

For simulating the forced response in the frequency range of interest, a 38-DOF PROM was generated from the full-order FEM (which has 208,753 DOF). The number of DOF and the

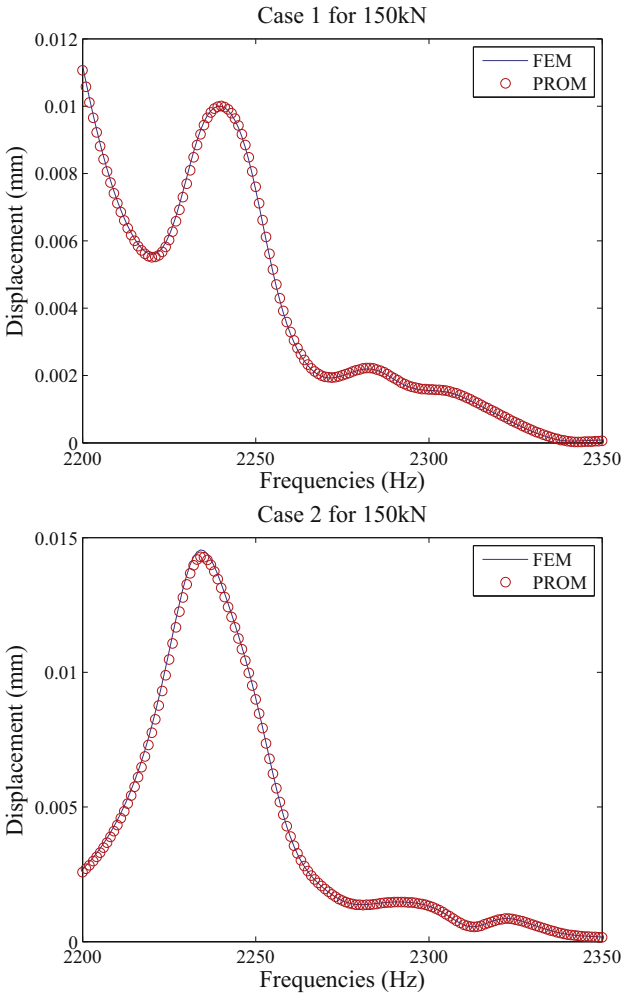

Fig. 9. Forced response predictions for the center node of the 5th cell (top) and the 9th cell (bottom) predicted by the FEM and a PROM for cases 1 (top) and 2 (bottom) with 150 kN prestress.

computational time required for the FEM and PROM are shown in Table 2. The reanalysis time for each variation is about 10,000 times shorter for the PROM compared to the FEM.

This computational gain would increase if a finer finite element mesh were used. That is because the PROM captures the low-dimensional physics of the problem. This low dimensionality means that relatively few coordinates are necessary to describe the dynamics of the actual physical system. This number of coordinates is a feature of the physics, not of the model used to discretize the physics. The finite element model will increase in size as the mesh is refined; however, the physics remains the same and are captured by the same PROM coordinates. Therefore, the computational savings from using the PROM are expected to be much greater for a more realistic FEM of an industrial battery pack.

As example cases for validating the accuracy of the PROM, two patterns of Young's modulus variations were applied to the cells, as shown in Table 1. In addition, for each variation pattern, prestress values of 150 kN and 470 kN were applied. Forced response simulations were then run by sweeping the excitation through the frequency range of interest for all four combinations of prestress values and variation patterns.

Figs. 9 and 10 shows the response of the center node of the 5th cell for variation pattern 1, and the 9th cell for variation pattern 2 under both 150 kN and 470 kN prestress. The solid lines indicate predictions

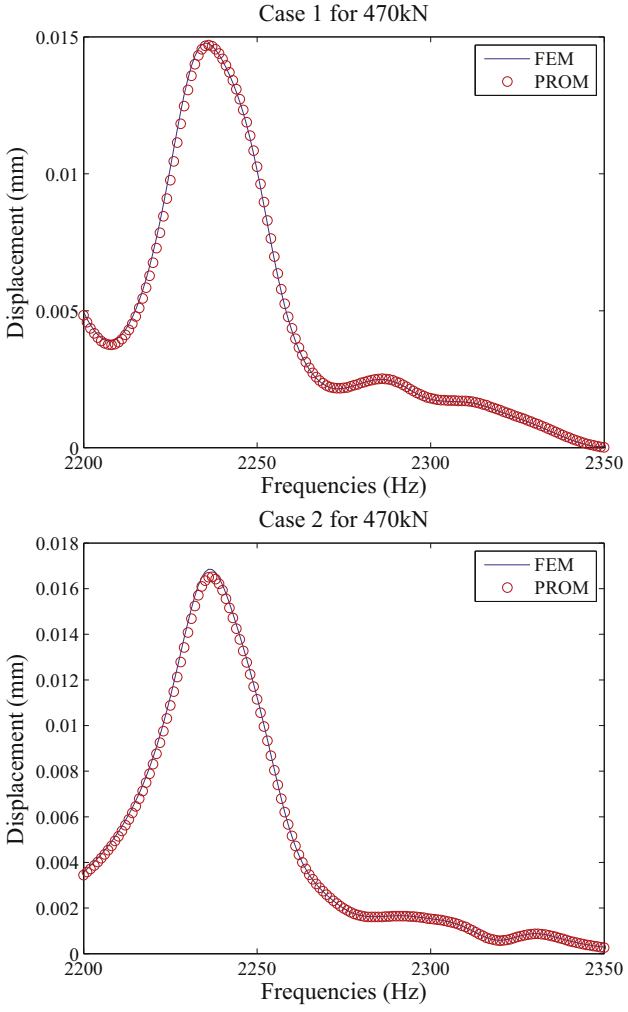

Fig. 10. Forced response predictions for the center node of the 5th cell (top) and the 9th cell (bottom) predicted by the FEM and a PROM for cases 1 (top) and 2 (bottom) with 470 kN prestress.

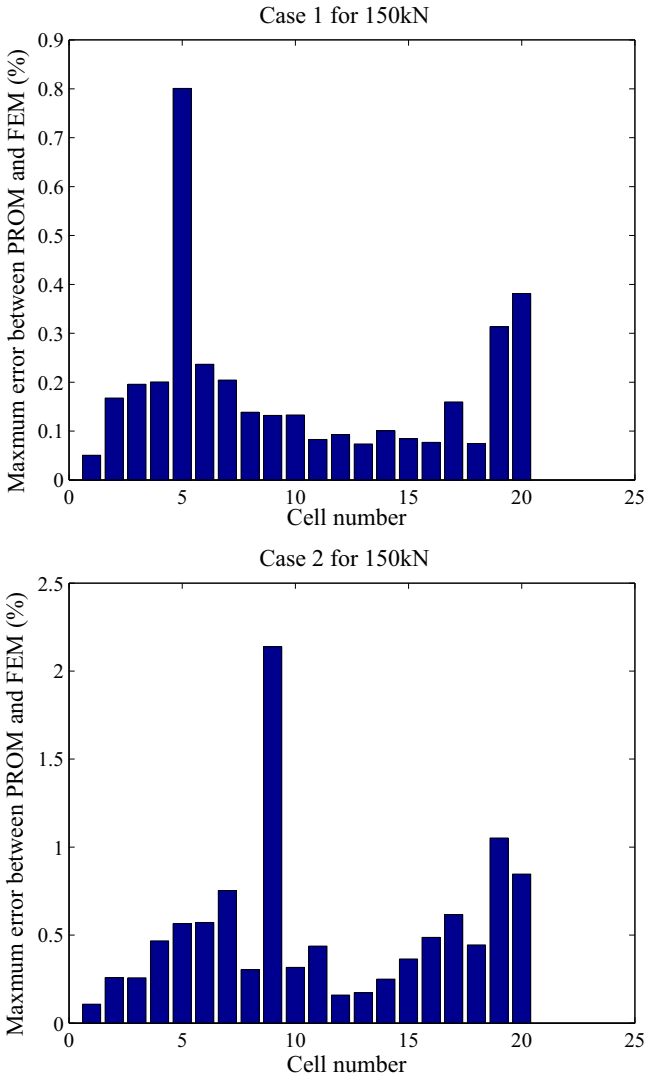

Fig. 11. Maximum errors between PROM and FEM for each cell (center node displacement) in the frequency range of interest for cases 1 (top) and 2 (bottom) with 150 kN prestress.

of full-order models and the symbols indicate PROM predictions. For all of these forced response simulations, it can be seen that the PROM results agreed very well with the much more expensive FEM results. Figs. 11 and 12 show the maximum error between the PROM and the FEM predictions for all 20 cells over the entire frequency range of interest. The maximum errors were no larger than 2.7%, and most were below 1% for all four simulation cases.

4.2. Effects of prestress for nominal system

Fig. 13 shows the maximum forced response amplitude in the frequency range 1500–3000 Hz for each cell in the nominal system. It is important to note that these amplitudes are the maximum values for the 1500–3000 Hz range, and the cells do not necessarily experience these amplitudes at the same excitation frequencies. The contributions from multiple system resonances may be represented in this plot. That is, these plots are not resonant response shapes. Rather, they are the baseline values for the maximum vibration response experienced by each cell in the nominal battery pack. They serve as a baseline for in the absence of cell-to-cell structural variations.

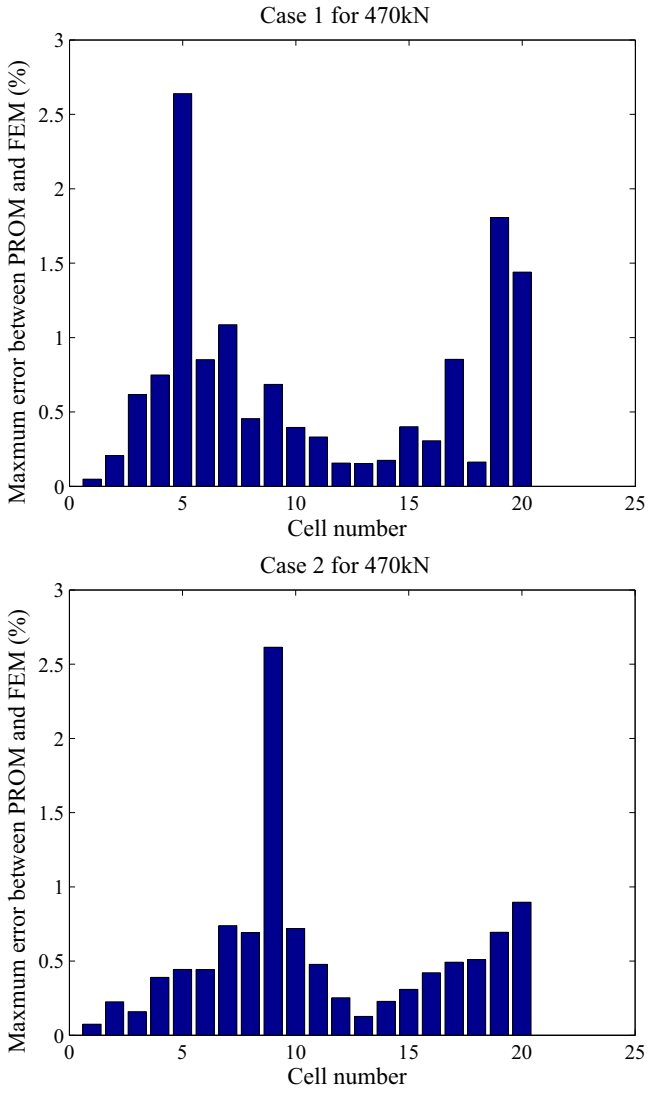

Fig. 12. Maximum errors between PROM and FEM for each cell (center node displacement) in the frequency range of interest for cases 1 (top) and 2 (bottom) with 470 kN prestress.

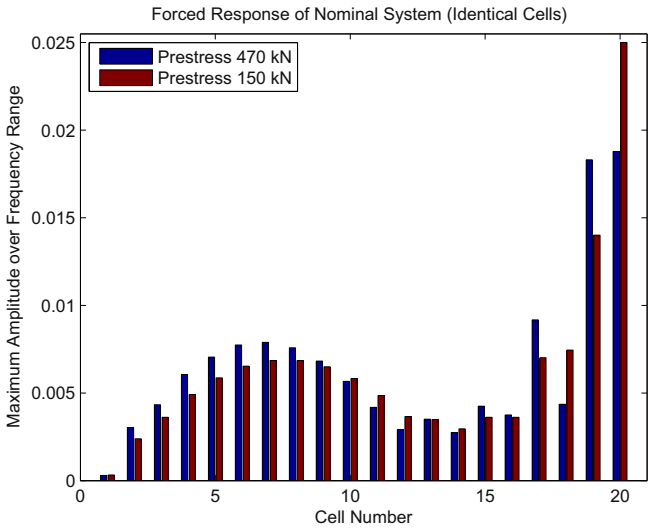

Fig. 13. Maximum forced response amplitudes for the nominal system.

These forced response simulation results are shown in Fig. 13 for two different prestress levels, 150 kN and 470 kN. It can be seen that the maximum amplitudes versus cell number show a similar trend. As expected, for both cases, the highest-responding cells are those closest to the excitation source. However, the different prestress levels lead to noticeable differences in the maximum amplitudes for these highest-responding cells.

It should be noted that the prestress level influences the strength of the structural coupling between cells. It is well known that the amount of Anderson localization in nearly periodic structures depends not only on the amount of structural variations but also on the strength of coupling [2,3]. Therefore, one would also expect to see different effects of structural variations for different prestress levels. This will be examined next.

4.3. Effects of prestress and structural variations

In a battery pack, a single cell with intense vibrations may lead to the failure of the entire pack. Thus, the maximum response level for any cell in a battery pack is a key reliability metric. However, in order to consider the effects of random structural variations, a probabilistic approach is needed. For example, a Monte Carlo simulation with thousands of variation patterns might be required. For a large FEM of an industrial battery pack, Monte Carlo simulations may be prohibitively expensive. In contrast, the accuracy and high computational speed of the PROM make it feasible to run Monte Carlo simulations.

In this study, Monte Carlo simulations were performed using the 38-DOF PROM to calculate the forced response for 10,000 different patterns of cell-to-cell elastic modulus variations. The variation patterns were sampled from a normal distribution with zero mean and standard deviation set to 5% of the nominal value. This corresponds to a standard deviation of approximately 2.5% with respect to the natural frequencies of the individual cells. As before, harmonic forcing was applied throughout the frequency range of 1500–3000 Hz, and prestress values of 150 kN and 470 kN were applied.

Fig. 14 shows the maximum forced response amplitude for each cell in the battery pack for a prestress level of 150 kN, both with and without structural variations. All of the amplitudes in this figure are normalized by the maximum amplitude of the nominal system. So a normalized amplitude of 1.0 (shown by the blue horizontal line) represents the maximum response level in the absence of cell-to-cell variations. For the system with cell-to-cell variations included, the maximum response was first obtained for each cell across the entire frequency range of interest for each Monte Carlo realization. Then, the maximum value among all 10,000 realizations was taken. The red bars plotted in Fig. 14 therefore represent the worst-case forced response amplitudes for each cell, and the horizontal red line illustrates the maximum response level with structural variations. It can be seen that effects of cell-to-cell variations lead to higher response levels for all cells. The increase is quite dramatic for some of the cells. However, the increase for the largest-responding cell was only about 10%.

Fig. 15 shows the results for the same simulations as in Fig. 14, except with the prestress level set to 470 kN. Again, the structural variations led to a higher response for every cell. Furthermore, there was an increase of over 40% for the largest-responding cell. Therefore, for this prestress level, neglecting the cell-to-cell variations might lead to a serious underprediction of the maximum stress, and thus an overprediction of the battery pack reliability.

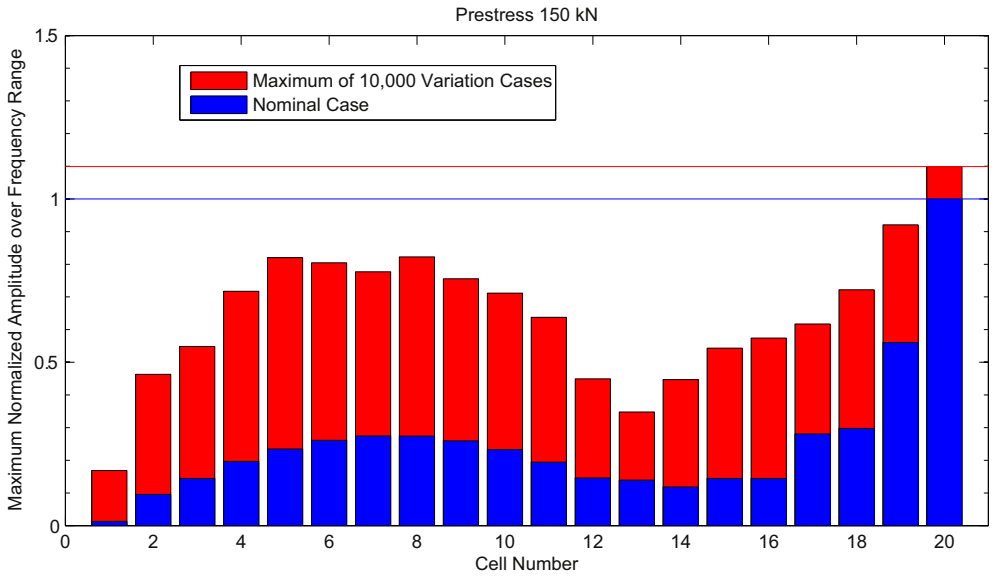

Fig. 14. Maximum normalized forced response amplitudes, prestress 150 kN.

As mentioned earlier, when there is no variation among the cells, the battery pack is a periodic structure. However, when the cells have variation in Young's modulus, the disorder in the structure can lead to localization, in which the vibration energy becomes concentrated in one or more cells. This confinement of energy leads to an increase in the forced response. Thus, it is important to investigate the effects of variations among the cells in order to estimate the increase in maximum forced response—as well as the attendant decrease in fatigue life—for an HEV battery pack.

5. Conclusions and discussion

There is currently a lot of research interest in hybrid electric vehicle (HEV) battery performance. However, relatively little attention has been paid to the structural dynamics of HEV battery packs. In this paper, the structural dynamic characteristics of HEV battery packs were explored using a simple but representative academic model of a battery pack with 20 pouch cells. It was shown that the structural dynamic characteristics are significantly affected by the prestress level used for joining cells within the pack. Also, it was shown that the dynamic response of the structure can be sensitive to small structural variations among the battery cells, because the system is a nominally periodic structure that features high modal density.

Thus, to predict the fatigue life for such a system, statistical calculations should be performed that account for the cell-to-cell structural variations. However, a structural finite element model of a full HEV battery could easily have millions of degrees of freedom. The large model size makes it cumbersome or infeasible to run Monte-Carlo-type simulations. Therefore, parametric reduced-order models (PROM) were derived to predict very quickly the structural dynamic response of HEV batteries with random cell-to-cell structural variations. First, previously developed PROM was applied to capture the different levels of prestress using a numerically stable transformation matrix and a third-order interpolation function. Second, to capture the cell-to-cell variation in the entire

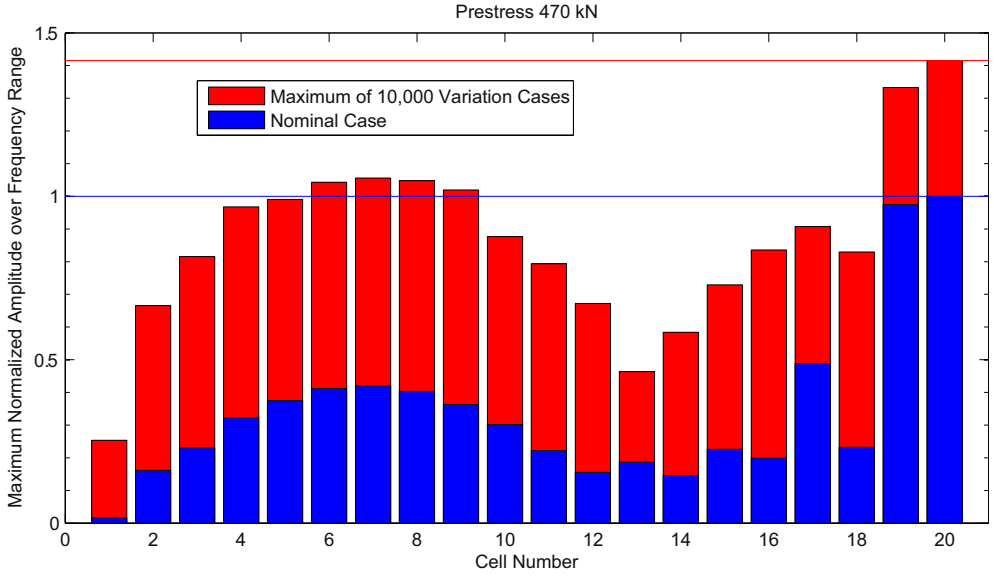

Fig. 15. Maximum normalized forced response amplitudes, prestress 470 kN.

battery pack, new PROM was introduced. The new PROM is based on two key assumptions: (1) mode shapes of the structure with variations can be represented as a linear combination of mode shapes of the structure with nominal parameters, and (2) variability in parameters in the corresponding cell can be captured by mode shapes of the nominal cell with its boundary displaced the same amount as the frame.

As a numerical example, a 38-DOF PROM was generated based on the FEM of the academic battery pack that has over 200,000 DOF. The forced response results from the PROM were found to match very well with those from the much larger FEM while reducing the simulation time by a factor of 10,000. The results also showed that prestress and small local variations in the structural parameters of the cells can induce very large changes in the global response.

The main advantage of the PROM presented in this work is that it can be used to predict the dynamic response accurately relative to the parent FEM, but at a much lower computational cost. Thus, it is appropriate to use the full-order FEM as a benchmark for evaluating the performance of the PROM. One can expect that PROM performance should ultimately be validated by using an industrial battery pack, not using an academic battery pack. However, this is an initial study. Because the academic battery pack captures the basic topology and key dynamic characteristics of an industrial battery pack, it is a suitable numerical example for this initial investigation.

Although this is an initial study for an academic example of a battery pack, it serves to illustrate that large battery packs with many cells may be nominally periodic structures that are sensitive to the effects of small, random variations. In particular, they may exhibit Anderson localization and suffer from significant increases in maximum forced response amplitude and stress levels in some cells. In such cases, it is important to be aware of these issues and to analyze the effects of different prestress and variation levels as early in the design process as possible. The PROM introduced in this paper provides an efficient and useful analysis tool for this purpose.

Disclosure

Reference herein to any specific commercial company, product, process, or service by trade name, trademark, manufacturer, or otherwise, does not necessarily constitute or imply its endorsement, recommendation, or favoring by the United States Government or the Department of the Army (DoA). The opinions of the authors expressed herein do not necessarily state or reflect those of the United States Government or the DoA, and shall not be used for advertising or product endorsement purposes.

UNCLASSIFIED: Distribution A. Approved for public release.

Acknowledgments

The authors gratefully acknowledge the financial support of the Automotive Research Center, a U.S. Army Center of Excellence for Modeling and Simulation of Ground Vehicles led by the University of Michigan.

References

[1] P. Anderson, Phys. Rev. 109 (5) (1958) /1492–1505.
[2] C.H. Hodges, J. Sound Vibration 82 (3) (1982) 411–424.
[3] O. Bendiksen, Chaos Solitons Fractals 11 (10) (2000) 1621–1660.
[4] G. Offer, V. Yufit, D. Howey, B. Wu, N. Brandon, J. Power Sources 206 (2012) 383–392.
[5] X. Xiao, W. Wu, X. Huang, J. Power Sources 195 (2010) 7649–7660.
[6] E. Sahraei, R. Hill, T. Wierzbicki, J. Power Sources 201 (2012) 307–321.
[7] B. Kenney, K. Darcovich, D. MacNeil, I. Davidson, J. Power Sources 213 (2012) 391–401.
[8] M. Dubarry, N. Vuillaume, B.Y. Liaw, J. Power Sources 186 (2009) 500–507.
[9] W.C. Hurty, AIAA J. 3 (4) (1965) 678–685.
[10] R.R. Craig Jr., M.C.C. Bampton, AIAA J. 6 (7) (1968) 1313–1319.
[11] S. Rubin, AIAA J. 13 (8) (1975) 995–1006.
[12] R.M. Hintz, AIAA J. 13 (8) (1975) 1007–1016.
[13] R.R. Craig Jr., C.-J. Chang, AIAA J. 14 (11) (1976) 1633–1635.
[14] M.P. Castanier, Y.-C. Tan, C. Pierre, AIAA J. 39 (6) (2001) 1182–1187.
[15] W.-H. Shyu, J. Gu, G.M. Hulbert, Z.-D. Ma, Finite Elem. Anal. Des. 35 (2) (2000) 119–140.
[16] E. Balmés, Mech. Syst. Signal Process. 10 (4) (1996) 381–394.
[17] E. Balmés, F. Ravary, D. Langlais, in: Proceedings of IMAC-XXII: A Conference and Exposition on Structural Dynamics, Dearborn, MI, 2004 pp. IMAC-XXII-57.
[18] G. Zhang, M.P. Castanier, C. Pierre, in: Proceedings of the Sixth European Conference on Structural Dynamics, Paris, France, 2005, pp. 993–998.
[19] K. Park, G. Zhang, M.P. Castanier, C. Pierre, in: Proceedings of ASME International Mechanical Engineering Congress and Exposition, Chicago, IL, USA, 2006 pp. IMECE2006-15069.
[20] K. Park, Component-based Vibration Modeling Methods for Fast Reanalyses and Design of Complex Structures (Ph.D. thesis), University of Michigan, 2008.
[21] S.K. Hong, B.I. Epureanu, M.P. Castanier, D.J. Gorsich, J. Sound Vibration 330 (2011) 1091–1110.
[22] S.K. Hong, B.I. Epureanu, M.P. Castanier, Mech. Syst. Signal Process. 37 (2013) 403–421.
[23] S.H. Lim, R. Bladh, M.P. Castanier, AIAA J. 45 (9) (2007) 2285–2298.
[24] M.T. Yang, J.H. Griffin, J. Eng. Gas Turbines Power 123 (4) (2001) 893–900.